Arab J Sci Eng (2015) 40:1197–1203
DOI 10.1007/s13369-015-1611-3

RESEARCH ARTICLE - MECHANICAL ENGINEERING

Effect of Post-Treatment Techniques on Corrosion and Wettability of Hydroxyapatite-Coated Co–Cr–Mo Alloy

Mostafa Rezazadeh Shirdar · Sudin Izman · Mohammad Mahdi Taheri · Mahtab Assadian · Mohammed Rafiq Abdul Kadir

Received: 14 November 2014 / Accepted: 4 February 2015 / Published online: 28 February 2015

Abstract This study is a comparison between the effect of sintering and alkaline post-treatment techniques on calcium phosphate-coated Co–Cr–Mo alloy in terms of electrochemical corrosion behavior and wettability. The Co–Cr–Mo substrates were electrophoretically coated by calcium phosphate in a solution of $Ca(NO_3) \cdot 4H_2O$ and $NH_4H_2PO_4$. The sintering and alkaline post-treatment techniques were then conducted to convert an as-deposited dicalcium phosphate dihydrate phase to crystalline hydroxyapatite (HA). The coated layers were characterized in terms of phase, crystallinity and composition using X-ray diffraction, Fourier transform infrared spectroscopy and energy-dispersive spectroscopy. In addition, morphology and thickness of coated layers were evaluated using a scanning electron microscope. The results indicate HA-coated samples with a sintering post-treatment technique exhibit more improvement in corrosion parameters, such as corrosion potential (E_{corr}) and corrosion current density (I_{corr}), but lower enhancement in hydrophilicity. However, the HA-coated samples with an alkaline post-treatment technique reveal higher hydrophilicity with lower improvement in corrosion resistance.

Keywords Co–Cr–Mo · Electrophoretic deposition (EPD) · Post-treatment · Corrosion · Wettability

M. R. Shirdar · S. Izman
Department of Manufacturing and Industrial Engineering, Faculty of Mechanical Engineering, Universiti Teknologi Malaysia, 81310 Skudai, Johor, Malaysia
e-mail: rsmostafa2@live.utm.my

S. Izman
e-mail: izman@mail.fkm.utm.my

M. M. Taheri · M. Assadian
Department of Materials Engineering, Faculty of Mechanical Engineering, Universiti Teknologi Malaysia, 81310 Skudai, Johor, Malaysia
e-mail: mtmohammad2@live.utm.my

M. Assadian
e-mail: mahtab.assadian@gmail.com

M. R. A. Kadir (✉)
Medical devices & Technology Group (MEDITEG), Faculty of Bioscience and Medical Engineering, Universiti Teknologi Malaysia (UTM), 81310 Skudai, Johor Bahru, Johor, Malaysia
e-mail: rafiq@biomedical.utm.my

1 Introduction

Cobalt chromium alloys have been used as orthopedic implants due to their wear resistance in vivo and superior stiffness compared to titanium alloys and stainless steels [1]. However, their use in hostile electrolytic environments, such as in human body fluid, is limited due to ion release [2], slow osseo-integration and lack of bioactivity [3]. The ion release and corrosion products can adversely affect the mechanical integrity and biocompatibility [4] and also lead to infection, swelling, loosening and local pain [5]. Coating the surface with hydroxyapatite, which is the main inorganic component of human bones and teeth, has been widely used to enhance its biocompatibility while maintaining its mechanical strength [6]. This non-conductive layer prevents ion exchange between the implant and its environment and consequently leads to increased corrosion resistance [7].

Other than resistance to corrosion, wettability of the implant surface also plays a crucial role in improving the clinical success rates of implantation [8]. Increasing surface wettability or hydrophilicity influences implant osseo-integration and bone formation by enhancing osteoblast maturation in vitro [9]. It can also affect the biological response to an implanted material through protein adsorption and

adhesion, platelet adhesion and activation, blood coagulation and cell and bacterial adhesion [10]. Wetting properties are affected by surface characteristics, such as surface topography and chemistry [8]. It has been reported that surface wettability was significantly higher in the HA-coated titanium sample compared to the non-coated titanium samples; this contrast is directly related to the difference in the surface chemistry of non-coated and HA-coated samples [11].

Although there are many methods, such as pulsed laser deposition [12], plasma spray [13], solgel [14] and electrophoretic deposition (EPD) [7,15–17], available to coat HA on metallic substrates, there are only two post-treatment methods that are commercially used: sintering post-treatment [15–17] and alkaline post-treatment [18–20]. Simple equipment, rapid formation and high efficiency have made EPD a preferable method for the coating of HA on biomaterials, such as stainless steel and titanium. Sintering post-treatment is then applied to convert dicalcium phosphate dehydrate (DCPD) to crystalline HA and also to minimize the porosity by increasing the coating density. In other biomaterials such as magnesium and its alloys, sintering post-treatment is not applicable due to the low melting point of the substrate after EPD process of HA. As an alternative, alkaline post-treatment is employed to transform the DCPD phase to crystalline HA.

Due to the increasing demand of the use of cobalt chromium alloys as biomedical devices and implant materials, this study embarks on the development of HA coating on Co–Cr–Mo using an EPD technique. Two post-treatment methods, including sintering and alkaline post-treatments, were then employed to modify the coating structure. The main aim of this research is to compare the effect of each post-treatment method on wettability and electrochemical corrosion behavior of this substrate.

2 Materials and Methods

2.1 Materials

A cylindrical bar of wrought Co–28Cr–6Mo alloy (ASTM F1537-94) [21] with a diameter of 10 mm. was cut into disks of 2 mm. thickness using a precision cutting machine. Samples were polished with abrasive silicon carbide papers (320, 600, 800 and 1200 grit) then ultrasonically cleaned with acetone for 10 min.

2.2 Electrophoretic Deposition

Electrolyte was prepared by mixing 0.42 mol/L $Ca(NO_3) \cdot 4H_2O$ and 0.25 mol/L $NH_4H_2PO_4$ [16] with the Ca/P ratio being 1.67 in DI water with the pH value of 3.5 adjusted by adding HNO_3 and $(CH_2OH)_3CNH_2$ [20]. The electrolyte was rendered homogeneous by continuously stirring at 100 rpm for 24 h. The EPD process was performed by a regulated DC power supply (DYY-6C, BEIJING LIUYI) in a current density of 9 mA/cm^2. The substrate, Co–Cr–Mo alloy, acted as the cathode, while a graphite electrode was used as the anode. Deposition was carried out in 20 min at room temperature (25 °C). After coating with the calcium phosphate, the specimens were removed from the electrolyte solution, rinsed in distilled water and dried at (60 °C) for 24 h. Two different post-treatment methods were then employed to convert dicalcium phosphate dihydrate (DCPD) to crystalline HA. The first as-deposited sample was sintered at (800 °C) for 1 h in the vacuum furnace at 10^{-5} torr [16], and the second one was immersed into the 0.1 mol/L NaOH solution at (70 °C) for 2 h [20]. After immersion, the samples were rinsed with distilled water and subsequently dried.

2.3 Electrochemical Corrosion and Wettability

In order to assess the corrosion behavior of non-coated and post-treated coated samples, potentiodynamic polarization studies were conducted using the potentiostat corrosion test machine (Princeton applied research, AMETEK, versaSTAT3). A three-electrode cell was used for electrochemical measurements, including a reference electrode [saturated calomel electrode (SCE)], counter electrode (graphite rod) and working electrode (the specimens). The tests were carried out in 500 mL of simulated body fluid (Kokubo solution [(mmol/L) 142 Na^+, 5 K^+, 2.5 Ca^{2+}, 1.5 Mg^{2+}, 4.2 HCO^{3-}, 147.8 Cl^-, 1 HPO_4^{2-}, 0.5 SO_4^{2-}]) with a pH of 7.6 and a temperature of (37 °C) [20]. The critical parameters, such as corrosion potential (E_{corr}) and corrosion current density (I_{corr}), were evaluated from the polarization curves.

The surface wettability of non-coated and HA-coated samples after each post-treatment method was evaluated by a water droplet contact angle-based test (VCA optima, AST) according to the ASTM D7334-08 standard [22]. A 1 ± 0.1 μL drop of water was utilized on the surface samples to measure the contact angles in a specified time (5 s). Five experiments were carried out for each of the samples.

3 Results and Discussion

3.1 Characterization

The surface morphology of the sintering post-treated samples is shown in Fig. 1a. The morphological feature reveals a regular flake-like structure diverging from the center toward the periphery after this post-treatment method. It has been reported that this morphological feature is beneficial for improvement in osseo-integration related to its efficiency of anchoring bone cells and promoting vascular and bone

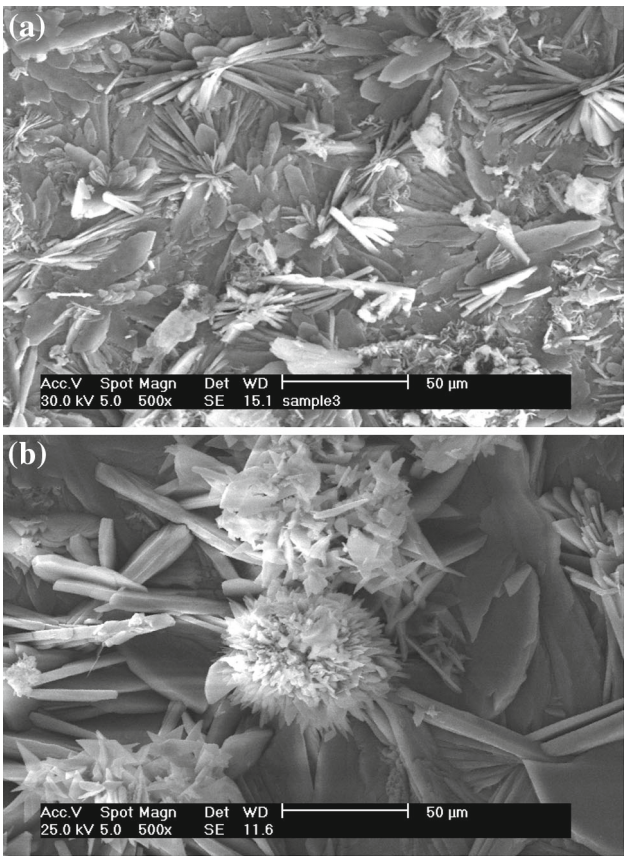

Fig. 1 SEM image of HA-coated Co–Cr–Mo after **a** sintering, **b** alkaline post-treatment

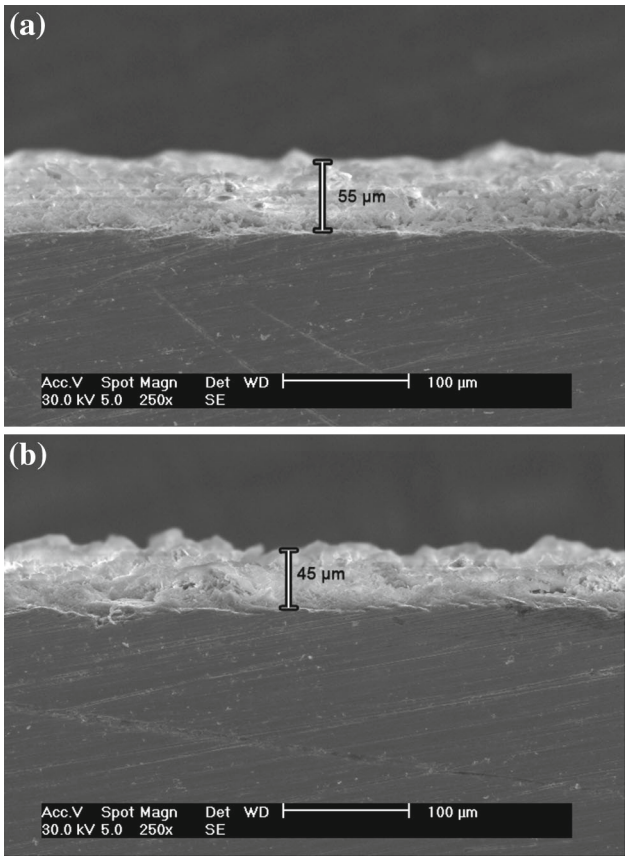

Fig. 2 Cross-sectional SEM image of HA-coated Co–Cr–Mo after **a** sintering, **b** alkaline post-treatment

tissue in-growth. Consequently, mechanical interlocking at the bone and implant interface would be enhanced with better bone growth [23]. Figure 1b shows the morphology of the coated sample within the alkaline post-treatment. A chrysanthemum-like structure with a solid core proved that HA crystals were grown in a radial way to construct this chrysanthemum flower morphological feature on the substrate surface. The cross-sectional SEM image of samples in Fig. 2a, b reveals that after both post-treatment methods, the HA-coated layer is relatively uniform with a thickness of about 55 µm for sintering and 45 µm for the alkaline post-treatment. The lower thickness of the alkaline post-treated sample is due to partial dissolution of DCPD resulting in the release of Ca^{2+} and PO_4^{3-} ions [22]. Figure 3a, b shows typical energy-dispersive spectroscopy (EDS) area analysis results of the sintered and alkaline post-treated sample, respectively. The Ca/P ratio of 1.57 and 1.59 confirms the formation of HA crystalline after both post-treatments. Dorozhkin has reported that the non-stoichiometric hydroxyapatite within $1.5 \leq \text{Ca/P} \leq 1.67$ has the same crystal structure and might be similarity described as a stoichiometric hydroxyapatite [24].

The X-ray diffraction (XRD) pattern of the as-deposited sample is shown in Fig. 4a. It is obvious from this pattern that the as-deposited coating is the mixture of HA and DCPD phases. Although the intensity of the DCPD phase is the highest, there are a few peaks related to crystalline HA. This result is in close agreement with the finding of Wen et al. [18].

Figure 4b shows the XRD pattern of the coated sample within the sintering post-treatment. This pattern confirms that most of the DCPD phase was transformed to the crystalline HA phases without detection of other apatite phases. This result is in close agreement with the finding of Eliaz et al. [17]. The XRD pattern of the coated sample within alkaline post-treatment is shown in Fig. 4c. This pattern reveals that regardless of the remaining small amounts of the DCPD phase, the mixture of HA and DCPD phases was transformed into HA crystalline by the alkaline solution. This result is also in close agreement with those of Wen et al. [18] and Song et al. [19].

Although both post-treatment methods transformed most of the DCPD phase to crystalline HA, the sharper peaks of crystalline HA in the XRD pattern of the sintered sample indicate that more crystallinity was obtained through this pre-treatment method. Although the difference is very small,

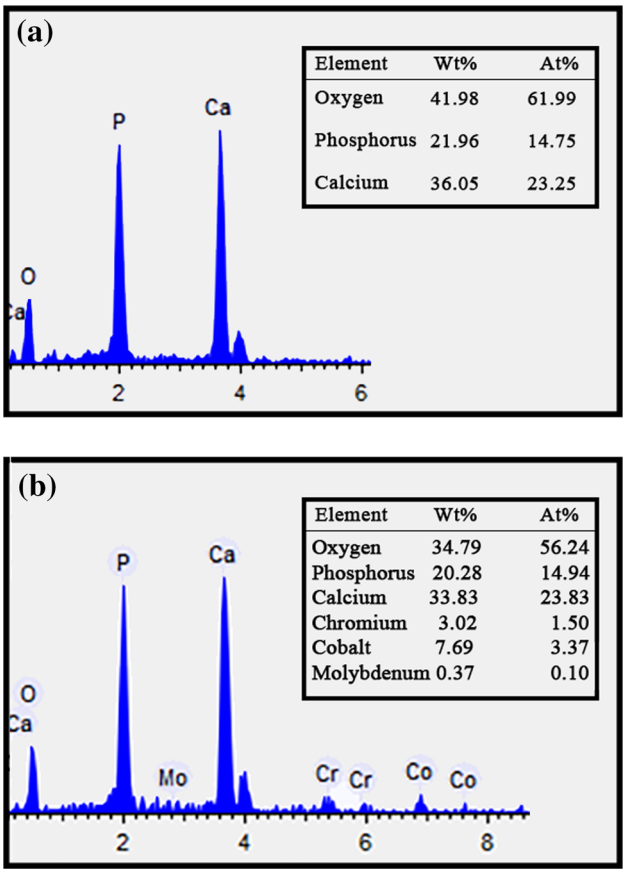

Fig. 3 EDS analysis of HA-coated Co–Cr–Mo after **a** sintering, **b** alkaline post-treatment

it is in close agreement with the EDS results which indicate that Ca/P ratio after sintering post-treatment is closer to the value of 1.67 rather than alkaline post-treatment. Both XRD and EDS results confirm that there is more crystalline HA after the sintering post-treatment.

Fourier transform infrared (FT-IR) spectroscopy (Thermo Scientific iD5 Diamond ATR 133, Nicolet iS5 FT-IR Spectrometer) was conducted to detect the chemical bonding in a spectral range of 500–4000 cm^{-1}. The FT-IR spectrum of the as-deposited sample is shown in Fig. 5a. PO bending is observed at 660 cm^{-1}, while P–O(H) stretching is found at 876 cm^{-1}. The bands at 1020, 1050 and 1127 cm^{-1} indicate the PO stretching, while O–H in-plane bending is observed at 1385 cm^{-1}. The band at 1637 cm^{-1} pertains to H_2O, while O–H stretching of water is observed at 3328, 3473 and 3518 cm^{-1}. The observations are in close agreement with those reported by Jamesh et al. [23]. The FT-IR spectrum confirms the formation of DCPD in the as-deposited sample.

Figure 5b shows the FT-IR spectrum of the sample within the sintering process at (800 °C); the O–H peaks became narrow, indicating the removal of some amount of hydroxyl component, such as water, from the crystalline structure. The bands observed at 875, 981, 1039 and 1091 cm^{-1} indicate the formation of a well-crystallized apatite in the FT-IR spectrum of the coated sample after the sintering process, which is in close agreement with the results reported by Meejoo et al. [25].

The FT-IR spectrum of the sample within the alkaline post-treatment is shown in Fig. 5c. The peak around 3400–3500 cm^{-1} is related to strongly absorbed or/and bound H_2O. The band at 3537 cm^{-1} is attributed to the O–H group, and the peak at 1640 cm^{-1} could correspond to the presence of water associated with HA. The formation of well-crystallized apatite within the alkaline post-treatment is recognized in the split bands particularly at 1112, 1052 and 1008 cm^{-1} which is in close agreement with the results reported by Jamesh et al. [23].

3.2 Electrochemical Corrosion Test

The potentiodynamic polarization tests were undertaken in a simulated body fluid (SBF) solution, and the related curves of non-coated and coated samples using different

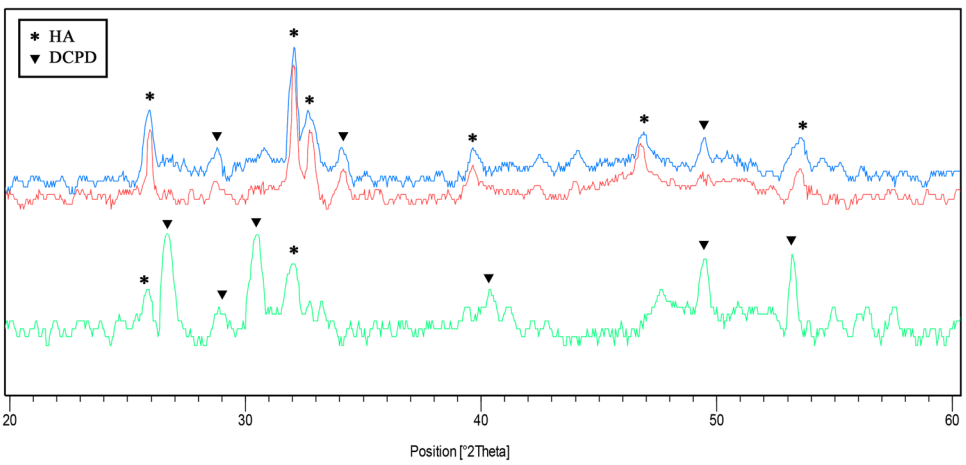

Fig. 4 X-ray diffraction patterns of samples **a** as-deposited, **b** sintering post-treatment, **c** alkaline post-treatment

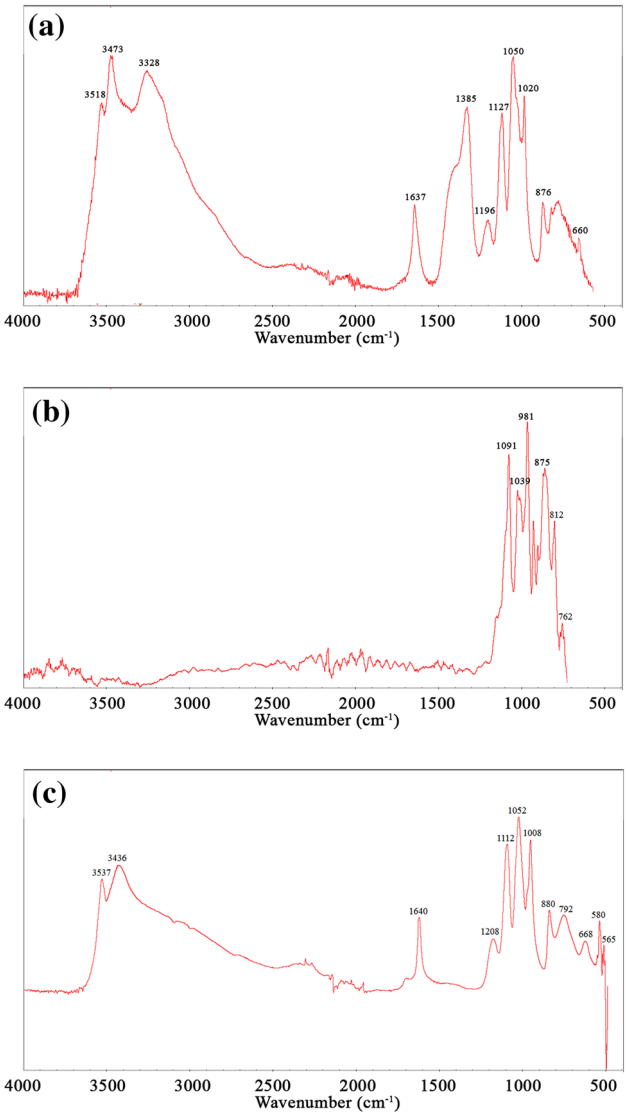

Fig. 5 FT-IR spectrum of sample **a** as-deposited, **b** sintering post-treated, **c** alkaline post-treated

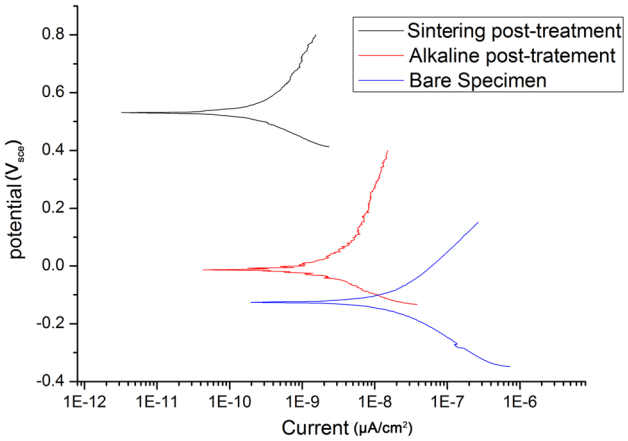

Fig. 6 Potentiodynamic polarization curves of bare specimen and post-treated samples

Table 1 Electrochemical corrosion test results

	Corrosion potential (V_{sce})	Corrosion current ($\mu A\,cm^{-2}$)
Bare specimen	−0.117	1.51E−7
Alkaline post-treatment	−0.01	1.42E−8
Sintering post-treatment	0.53	1.23E−9

post-treatments, in comparison, are given in Fig. 6. Both curves of post-treated samples exhibit a similar regime of bare material but with a different value of E_{corr} and I_{corr} which is summarized in Table 1. Corrosion current density (I_{corr}) is defined as the intersection between cathodic and the anodic linear extrapolations at corrosion potential (E_{corr}). This value is directly related to electrode potential, and it can provide more realistic results related to the electrochemical behavior of the material. Therefore, E_{corr} and I_{corr} values can provide more realistic results related to electrochemical behavior of the implants [26]. It can be clearly seen from Fig. 6 and Table 1 that compared to the bare sample, the E_{corr} of both alkaline and sintering post-treated samples has increased from −0.117 to −0.01 V_{sce} and 0.53V_{sce}, respectively. In addition, I_{corr} of both alkaline and sintering post-treated samples has increased from 1.51E−7 to 1.42E−8 $\mu A\,cm^{-2}$ and 1.23 E−9 $\mu A\,cm^{-2}$, respectively. Based on these results, the comparison of the corrosion resistance of these three samples is observed in the following order: sintering post-treatment > alkaline post-treatment > bare specimen. Results reveal that HA-coated sample with sintering post-treatment exhibits higher corrosion resistance than HA-coated sample with alkaline post-treatment. This possibly is related to the thicker coating layer and creation of a uniform and denser structure with more crystalline HA at a high temperature [7].

3.3 Contact Angle Measurement

In this study surface, wettability was evaluated by contact angle measurement. The hydrophilic and hydrophobic nature of bare specimen and coated samples within both post-treatment methods was determined by its water contact angle. As shown in Fig. 7, the water contact angle of the bare specimen surface is 118°. This indicates that this smooth surface is a hydrophobic surface and is not considered desirable for medical implants [27,28] since it could not promote an environment conducive to bone formation [8]. The HA-coated sample within the sintering post-treatment shows a lower water CA of 71° which demonstrates a significant improvement in surface wettability compared to the bare specimen. Rausch-fan et al. [29] and Zhao et al. [30] reported that the

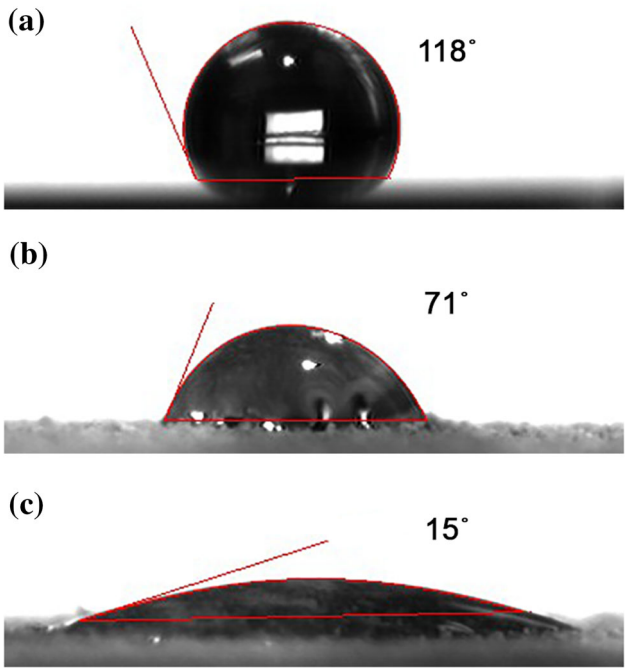

Fig. 7 Contact angle of water droplets measured on **a** bare specimen, **b** sintering, **c** alkaline post-treated samples

hydrophilic nature of implant surfaces strongly influences the cell differentiation and growth factor production. Therefore, it seems that the sintering post-treatment of the HA-coated sample possibly creates more a desirable surface for implant applications. The modified HA-coated sample within the alkaline post-treatment reveals a CA of 15° lower than the sintering post-treatment results. This is possibly related to the surface characteristics, such as surface topography, and the chemistry of the HA-coated layer. Therefore, it seems that the alkaline post-treatment creates a highly hydrophilic surface which plays a major role in tissue–implant interaction [31], early osseo-integration [15] and also bone formation [8].

4 Conclusion

This study developed EPD HA coating on Co–Cr–Mo alloy and compared the effect of sintering and alkaline post-treatment in terms of characterization, electrochemical corrosion behavior and wettability on this substrate. The following conclusions were drawn from the above experimental evidence:

1. It can be seen that HA coating on Co–Cr–Mo alloy via the EPD method provides a bioactive layer to increase the corrosion resistance of the substrate and provide a hydrophilic surface.
2. XRD analysis confirmed that the majority of the DCPD phases transformed to HA crystalline after both sintering and alkaline post-treatment. However, the comparison between two patterns indicates a higher percentage of crystallinity of HA within the sintering post-treatment.
3. SEM and EDS analyses confirmed the presence of densely packed uniform HA coating on the substrate after both post-treatment methods but with different morphology. The sintering post-treatment produced regular flake-like structures which are beneficial for the improvement of osseo-integration, while the alkaline post-treatment produced chrysanthemum-like structures.
4. The FT-IR spectrum of the as-deposited sample confirmed the formation of DCPD phases after EPD coating, and the FT-IR spectrum of both sintering and alkaline post-treated samples indicated the formation of a well-crystallized apatite.
5. Compared with the non-coated Co–Cr–Mo sample, E_{corr} and I_{corr} as well as the corrosion resistance of both coated samples with alkaline and sintering post-treatment increased. However, this increase is more significant for the sintering post-treated sample possibly due to its thicker coating layer and higher amount of crystalline HA.
6. A lower contact angle of the alkaline post-treated substrate (15°) compared to the sintering post-treated substrate (71°) reveals that the alkaline post-treatment produced more hydrophilic surface.

References

1. Rahaman, M.N.; Yao, A.; Bal, B.S.; Garino, J.P.; Ries, M.D.: Ceramics for prosthetic hip and knee joint replacement. J. Am. Ceram. Soc. **90**(7), 1965–1988 (2007)
2. Zeh, A.; Planert, M.; Siegert, G.; Lattke, P.; Held, A.; Hein, W.: Release of cobalt and chromium ions into the serum following implantation of the metal-on-metal Maverick-type artificial lumbar disc (Medtronic Sofamor Danek). Spine **32**(3), 348–352 (2007)
3. Plecko, M.; Sievert, C.; Andermatt, D.; Frigg, R.; Kronen, P.; Klein, Ka.; Stübinger, S.; et al.: Osseointegration and biocompatibility of different metal implants—a comparative experimental investigation in sheep. BMC Musculoskelet. Disord. **13**(1), 32 (2012)
4. Mohedano, M.; Matykina, E.; Arrabal, R.; Pardo, A.; Merino, M.C.: Metal release from ceramic coatings for dental implants. Dent. Mater. **30**, e28–e40 (2014)
5. Aksakal, B.; Gavgali, M.; Dikici, B.: The effect of coating thickness on corrosion resistance of hydroxyapatite coated Ti6Al4V and 316L SS implants. J. Mater. Eng. Perform. **19**(6), 894–899 (2010)
6. Sarkar, A.; Kannan, S.: In situ synthesis, fabrication and Rietveld refinement of the hydroxyapatite/titania composite coatings on 316L SS. Ceram. Int. **40**(5), 6453–6463 (2014)
7. Assadian, M.H.; Jafari, S.M.; Ghaffari Shahri, M.H.; Idris, Gholampour, B.: Corrosion resistance of EPD nanohydroxyapatite coated 316L stainless steel. Surface Eng. **30**(11), 806–813 (2014)
8. Rupp, F.; Gittens, R.A.; Scheideler, L.; Marmur, A.; Boyan, B.D.; Schwartz, Z.; Geis-Gerstorfer, J.: A review on the wetta-

bility of dental implant surfaces I: theoretical and experimental aspects. Acta Biomater. **10**(7), 2894–2906 (2014)
9. Gittens, R.A.; Olivares-Navarrete, R.; Cheng, A.; Anderson, D.M.; McLachlan, T.; Stephan, I.; Geis-Gerstorfer, J.; et al.: The roles of titanium surface micro/nanotopography and wettability on the differential response of human osteoblast lineage cells. Acta Biomater. **9**(4), 6268–6277 (2013)
10. Xu, L.-C.; Siedlecki, C.A.: Effects of surface wettability and contact time on protein adhesion to biomaterial surfaces. Biomaterials **28**(22), 3273–3283 (2007)
11. Rad, A.T.; Solati-Hashjin, M.; Osman, N.A.A.; Faghihi, S.: Improved bio-physical performance of hydroxyapatite coatings obtained by electrophoretic deposition at dynamic voltage. Ceram. Int. **40**(8), 12681–12691 (2014)
12. Carradò, A.: Nano-crystalline pulsed laser deposition hydroxyapatite thin films on Ti substrate for biomedical application. J. Coat. Technol. Res. **8**(6), 749–755 (2011)
13. Enayati, M.H.; Fathi, M.H.; Zomorodian, A.: Characterisation and corrosion properties of novel hydroxyapatite niobium plasma sprayed coating. Surf. Eng. **25**(4), 338–342 (2009)
14. Esfahani, H.; Dabir, F.; Taheri, M.; Sohrabi, N.; Toroghinejad, M.R.: Sol–gel derived hydroxyapatite coating on TiB2/TiB/Ti substrate. Surf. Eng. **28**(7), 526–531 (2012)
15. Jain, P.; Mandal, T.; Prakash, P.; Garg, A.; Balani, K.: Electrophoretic deposition of nanocrystalline hydroxyapatite on Ti6Al4V/TiO_2 substrate. J. Coat. Technol. Res. **10**(2), 263–275 (2013)
16. Bhawanjali, S.; Revathi, A.; Popat, K.C.; Geetha, M.: Surface modification of Ti–13Nb–13Zr and Ti–6Al–4V using electrophoretic deposition (EPD) for enhanced cellular interaction. Mater. Technol. Adv. Biomater. **29**(B1), B54–B58 (2014)
17. Eliaz, N.; Sridhar, T.M.; Kamachi Mudali, U.; Raj, B.: Electrochemical and electrophoretic deposition of hydroxyapatite for orthopaedic applications. Surf. Eng. **21**(3), 238–242 (2005)
18. Wen, C.; Guan, S.; Peng, L.; Ren, C.; Wang, X.; Hu, Z.: Characterization and degradation behavior of AZ31 alloy surface modified by bone-like hydroxyapatite for implant applications. Applied Surface Science **255**(13), 6433–6438 (2009)
19. Song, Y.; Zhang, S.; Li, J.; Zhao, C.; Zhang, X.: Electrodeposition of Ca–P coatings on biodegradable Mg alloy: in vitro biomineralization behavior. Acta Biomater. **6**(5), 1736–1742 (2010)
20. Bakhsheshi-Rad, H.R.; Idris, M.H.; Abdul-Kadir, M.R.: Synthesis and in vitro degradation evaluation of the nano-HA/MgF_2 and DCPD/MgF_2 composite coating on biodegradable Mg–Ca–Zn alloy. Surf. Coat. Technol. **222**, 79–89 (2013)
21. ASTM F1537-94.: Standard Specification for Wrought Cobalt–Chromium–Molybdenum Alloy for Surgical Implant applications. Annual Book of ASTM Standards: Medical Devices and Services, vol. 13.01, pp. 865–867. American Society for Testing and Materials, Philadelphia, PA (1995)
22. American Society for Testing and Materials (ASTM) D7334-08.: Standard Practice for Surface Wettability of Coatings Substrates and Pigments by Advancing Contact Angle Measurement. ASTM International, West Conshohocken, PA (2013)
23. Jamesh, M.; Kumar, S.; Sankara, T.S.N.N.: Electrodeposition of hydroxyapatite coating on magnesium for biomedical applications. J. Coat. Technol. Res. **9**(4), 495–502 (2012)
24. Dorozhkin, S.V.: A review on the dissolution models of calcium apatites. Prog. Cryst. Growth Charact. Mater. **44**(1), 45–61 (2002)
25. Meejoo, S.; Maneeprakorn, W.; Winotai, P.: Phase and thermal stability of nanocrystalline hydroxyapatite prepared via microwave heating. Thermochim. Acta **447**(1), 115–120 (2006)
26. Galvele, J.R.: Tafel's law in pitting corrosion and crevice corrosion susceptibility. Corros. Sci. **47**(12), 3053–3067 (2005)
27. Junker, R.; Dimakis, A.; Thoneick, M.; Jansen, J.A.: Effects of implant surface coatings and composition on bone integration: a systematic review. Clin. Oral Implants Res. **20**(4), 185–206 (2009)
28. Schwarz, F.; Ferrari, D.; Herten, M.; Mihatovic, I.; Wieland, M.; Sager, M.; Becker, J.: Effects of surface hydrophilicity and microtopography on early stages of soft and hard tissue integration at nonsubmerged titanium implants: an immunohistochemical study in dogs. J. Periodontol. **78**(11), 2171–2184 (2007)
29. Rausch-fan, X.; Qu, Z.; Wieland, M.; Matejka, M.; Schedle, A.: Differentiation and cytokine synthesis of human alveolar osteoblasts compared to osteoblast-like cells (MG63) in response to titanium surfaces. Dent. Mater. **24**(1), 102–110 (2008)
30. Zhao, G.; Raines, A.L.; Wieland, M.; Schwartz, Z.; Boyan, B.D.: Requirement for both micron- and submicron-scale structure for synergistic responses of osteoblasts to substrate surface energy and topography. Biomaterials **28**(18), 2821–2829 (2007)
31. Le Guéhennec, L.; Soueidan, A.; Layrolle, P.; Yves, A.: Surface treatments of titanium dental implants for rapid osseointegration. Dent. Mater. **23**(7), 844–854 (2007)